

Whole-Body Diffusion-Weighted MRI of the Bone Marrow in Health and Disease

Anwar R. Padhani¹; Hassan Douis²; Peter Gall³

¹Paul Strickland Scanner Centre, Mount Vernon Cancer Centre, Northwood, Middlesex, UK

²Department of Radiology, Royal Orthopaedic Hospital, Birmingham, UK

³Siemens Healthcare, Erlangen, Germany

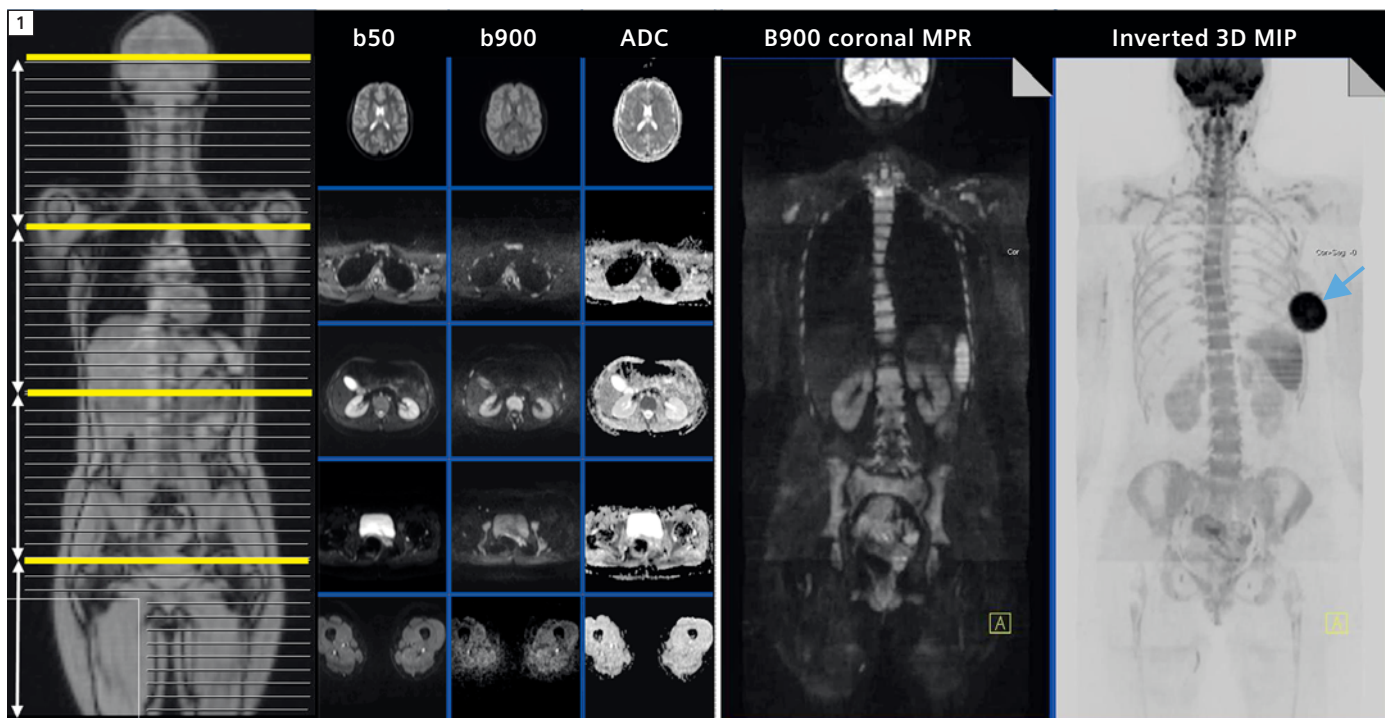
Background

A comprehensive imaging assessment of the skeletal bone marrow requires a multimodal approach because no one technique is able to evaluate all aspects of bone health. Thus, ^{99m}Tc-MDP skeletal scintigraphy and ¹⁸F-Na PET evaluate osteoblastic function, ultrashort TE and CT scans evaluate the structural properties of bone and the osteolytic activity of osteoclasts. Non-specific PET tracers can evaluate bone marrow/tumor membrane transporters and metabolism. Relevant

tracers include ¹⁸F-fluorodeoxyglucose (FDG) for glucose metabolism, ¹¹C/¹⁸F-thymidine (FLT) for DNA synthesis, ¹¹C/¹⁸F-acetate for fatty acid synthesis, ¹¹C-methionine for protein synthesis and ¹¹C/¹⁸F-choline for cell membrane synthesis and degradation [1]. Tumor specific tracers include ¹⁸F-FES (fluoro-estradiol for breast cancer), ¹⁸F-FDHT (fluorodihydrotestosterone for prostate cancer) and engineered antibody fragments that target tumor cell-surface targets such as HER-2/neu (for breast

cancer) and prostate specific membrane antigen (PSMA) [2]. Dynamic contrast-enhanced MRI (DCE-MRI) can evaluate the vascularisation of bone marrow and its cellular content can be assessed using Dixon and diffusion MRI techniques. These techniques have variable clinical availability and whole-body imaging capability.

In recent years, whole-body MRI has emerged as an excellent imaging modality for the evaluation of normal bone, of bone marrow infiltration and the detec-



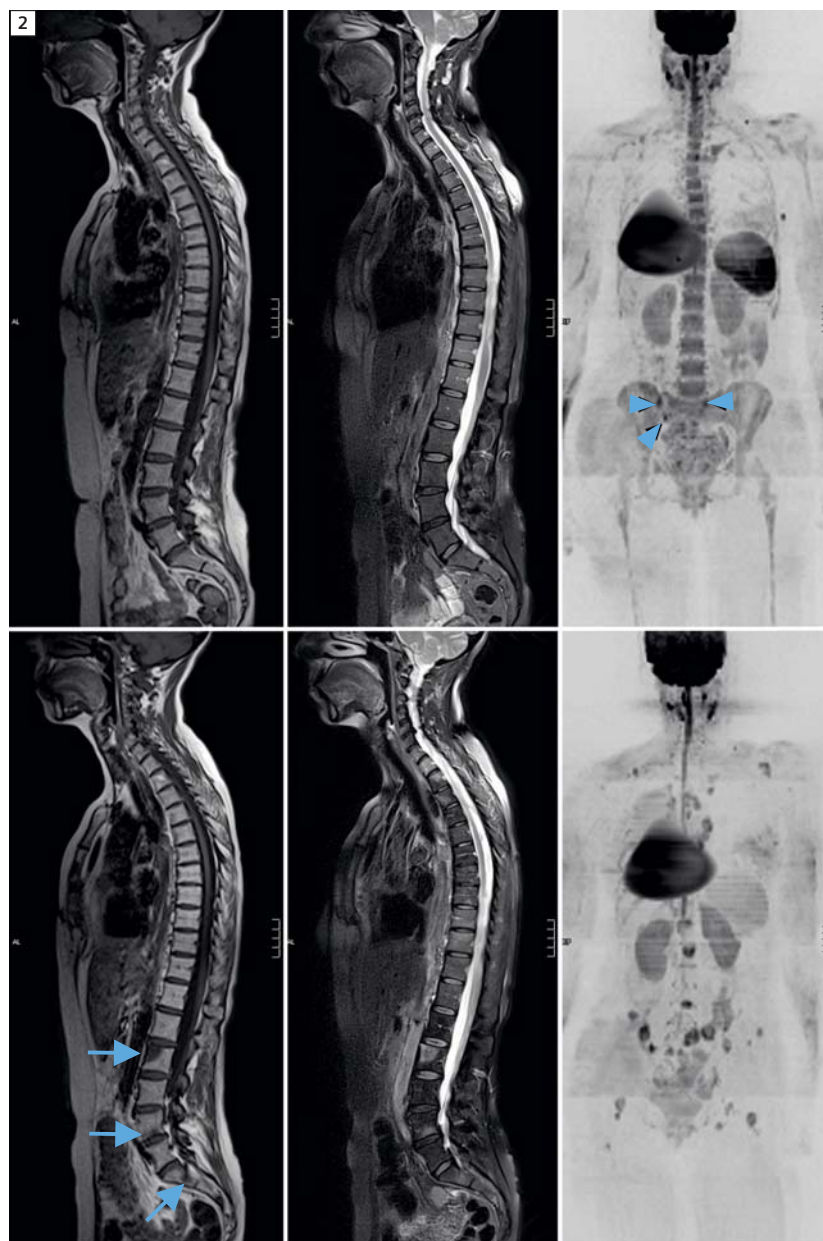
1 WB-DWI workflow. 27-year-old-woman with sarcomatoid left breast cancer (arrow). The bone marrow pattern is normal for this age. Axial DWI from the skull base to the mid-thigh is performed using 2 b-values (50 and 900 s/mm²) with a slice thickness of 5 mm in 4 stations. The b900 images are reconstructed into the coronal plane (5 mm) and displayed as thick 3D MIPs (inverted grey scale). ADC images are computed inline with mono-exponential fitting of b50 and b900 signal intensities.

tion of skeletal metastases due to its exquisite soft tissue contrast, high spatial resolution and lack of ionizing radiation [3]. Whole-body MRI is particularly attractive for children* and young adults because it lacks ionizing radiation. Despite its high sensitivity and high specificity for the detection of skeletal metastases, whole-body MRI has not been widely adopted into daily clinical practice. This is predominantly due to the fact, that whole-body MRI performed with conventional sequences has to be tailored for each tumor type, has long examination times, often requires the administration of intravenous contrast and importantly, it is time consuming to analyse and report [4]. However, there is a strong clinical need for whole-body tumor assessments particularly for cancer patients.

Whole-body diffusion-weighted MRI (WB-DWI) is a new powerful adjunct to anatomical whole-body MRI because it provides a functional assessment of disease burden, can quantify disease extent, does not require the administration of exogenous contrast medium and can be performed in reasonably short examination times. Furthermore, WB-DWI can improve the reading and test performance of anatomical whole-body MR examinations because areas of increased cellularity are depicted as regions of high signal-intensity, therefore allowing an 'at-a-glance' assessment of disease burden and distribution [5]. Whole-body DWI is emerging as a particularly promising imaging technique in the detection, assessment of extent and therapy monitoring of skeletal metastases [6] because it is sensitive to bone marrow cellularity, the relative proportion of fat and marrow cells, water content and bone marrow perfusion.

Technique of whole-body DWI

Most modern high-field MRI systems possess echo-planar and parallel imaging capabilities and allow the use of high-performance gradients which together with phased-array multichannel surface coils, make it feasible for WB-DWI to be implemented into clinical practice. Currently we find that WB-DWI

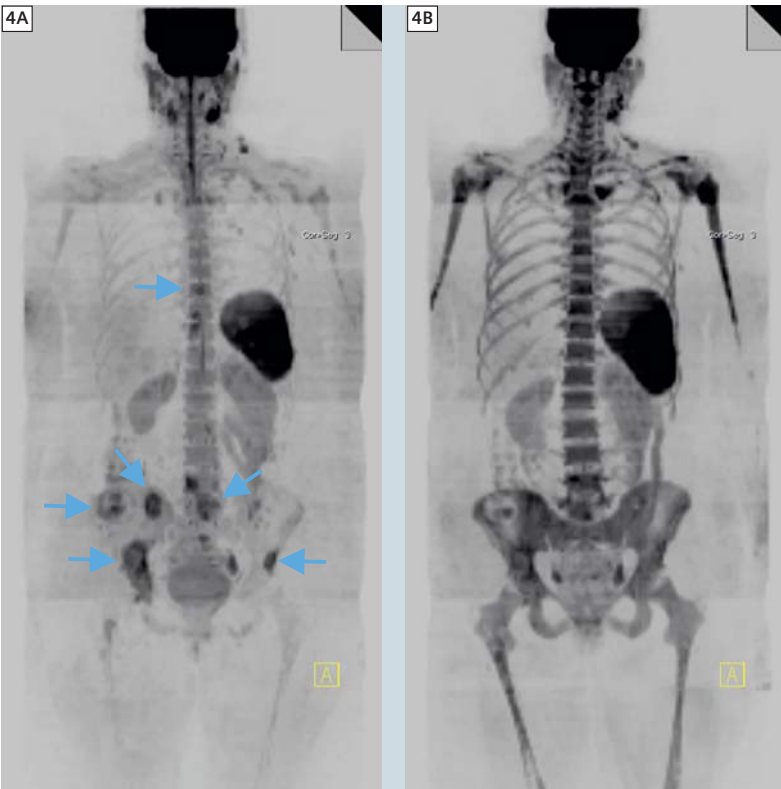


2 Bone marrow hypoplasia due to chemotherapy with disease progression. 49-year-old woman with metastatic breast cancer before and after 3 cycles of carboplatin chemotherapy. Both rows left-to-right: spine T1-weighted spin-echo, spine T2-weighted spin-echo with spectral fat saturation and b900 3D MIP (inverted scale) images. Top row before chemotherapy shows normal background bone marrow pattern with superimposed small volume bone metastases (arrow heads). Bottom row after chemotherapy shows marked disease progression with enlarging and new bony metastases (arrows). Note that bone marrow hypoplasia has developed in the ribs, spine and pelvis. Note reductions of signal intensity of the spleen secondary to iron deposition due to blood transfusions. There is a right sided silicone containing breast enhancement bra pad in place on both examinations.

*MR scanning has not been established as safe for imaging fetuses and infants under two years of age. The responsible physician must evaluate the benefit of the MRI examination in comparison to other imaging procedures.



3 Bone marrow hypoplasia due to aromatase inhibitor therapy. 56-year-old post-menopausal woman with estrogen receptor positive breast cancer on long term anastrozole therapy. Long term therapy of aromatase inhibitors such as anastrozole put women at greater risk for of osteoporosis which in turn leads to increased bone marrow fat. Left-to-right: spinal T1-weighted GRE sequence (from the scout views), T1-weighted spin-echo, T2-weighted spin-echo with spectral fat saturation and b900 3D MIP (inverted scale) images. There is some loss of vertebral height of the D9 vertebral body. Note the visibility of the entire length of the spinal cord on the 3D inverted MIP images and ready visibility of the dorsal nerve root ganglia of the brachial and lumbar plexuses. Focal high-signal lesions over the left chest are due to an acneiform rash on the skin.



4 Bone marrow hyperplasia induced by chemotherapy with G-CSF therapy. 50-year-old woman with metastatic breast cancer before and after 3 cycles of erubulin chemotherapy with growth-colony stimulating factor (G-CSF) given to prevent neutropenia. b900 3D MIP (inverted scale) images. Left image show multiple bone metastases (arrows). Right image after 3 cycles of chemotherapy shows increases in signal intensity of the bone marrow leading to the decreased visibility of the bone metastases. The splenic size has also increased. The increased signal intensity of the background bone marrow should not be misinterpreted as malignant progression.

is best performed at 1.5T using multiple surface coils for signal reception which allows uniform fat-suppression over large fields-of-view. Although imaging at 3T increases the signal-to-noise ratio, WB-DWI remains challenging because of increased susceptibility artifacts and poorer fat suppression.

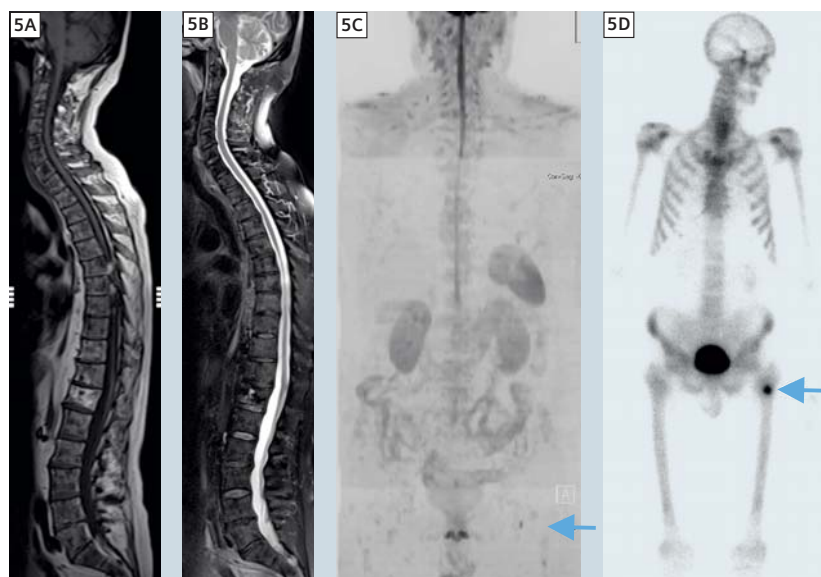
A multiple-averaged, free-breathing technique is most commonly used for data acquisition. In general, the use of two diffusion sensitizing gradients is sufficient to enable good quality, clinically useable images to be acquired. Low b-value black-blood (50 s/mm^2) combined with high b-value ($800\text{--}1000 \text{ s/mm}^2$) images are used in combination for anatomic depiction, disease detection and for the calculation of apparent diffusion coefficient (ADC) values [5, 7]. Our preferred method for fat suppression uses inversion recovery because it allows uniform fat suppression over large fields-of-view [8].

Our institutional protocol combines whole-body MRI and whole-body DWI done on a 1.5T MAGNETOM Avanto scanner (Siemens Healthcare, Erlangen, Germany) equipped with a continuous moving table option and total imaging matrix (Tim) body surface coils. First, conventional sagittal T1-weighted and T2-weighted fat-suppressed images of the spine are obtained. Subsequently, axial T1-weighted and STIR images from the skull vault to the mid-thigh are acquired using continuous table movement employing multiple breath-holds for image acquisitions of the chest, abdomen, pelvis and upper thighs. Axial DWI from the skull vault to the mid-thigh is then performed using b-values of 50 s/mm^2 and a b-value of 900 s/mm^2 with a slice thickness of 5 mm. The axial DWI acquisition is usually achieved in 4 contiguous stations using a free-breathing technique, with each station taking approximately 6 minutes to acquire. The high b-value images are then reconstructed in orthogonal planes as thin multiplanar reconstructions (5 mm) and as thick 3D maximum intensity projections (MIPs) which are usually displayed using an inverted grey scale. ADC maps are computed inline with system soft-

ware using mono-exponential fitting in which each voxel reflects the tissue diffusivity (units: $\mu\text{m}^2/\text{s}$) (Fig. 1).

Bone marrow imaging on WB-DWI

In order to be able to utilize WB-DWI in the detection, characterization and treatment assessment of skeletal metastases, it is vital to be familiar with the signal distribution of normal bone marrow on high b-value images. Normal adult bone marrow distribution becomes established by the age of 25 years with mixed red bone marrow found in the axial skeleton, the humeral and femoral proximal metaphyses whilst yellow marrow is found in the appendicular skeleton. Thereafter, conversion of red marrow regions to yellow marrow occurs at a slow rate, the speed of conversion being dependent on patient gender and underlying medical conditions [9]. It is thought that the reduced water content [9], the larger-sized fat cells, the hydrophobic nature of fat and poorer perfusion all contribute to lower signal intensities and ADC values of the yellow bone marrow. On the other hand, with increasing cellularity and water content and greater perfusion, mixed yellow-red bone marrow returns higher signal intensities and paradoxically higher ADC values [5, 10–12]. The changing distribution of the normal marrow is exquisitely demonstrated on WB-DWI (Fig. 1). Similarly, both bone marrow hypo- and hypercellularity are also well depicted on WB-DWI. Common causes for bone marrow hypocellularity include chemotherapy (Fig. 2), radiotherapy, myeloproliferative disorders (e.g. myelofibrosis, myelodysplasia), non-malignant marrow disorders (e.g. aplastic anemia), old age and osteoporosis (including drug induced), chronic disease (e.g. renal failure, chronic liver disease, rheumatoid arthritis) and prolonged immobility. In contrast, relative bone marrow hypercellularity is observed in children and adolescents, chronic anaemia, in smokers, chronic cardiac failure, in pregnancy and in patients treated with hematopoietic growth factors such as granulocyte-colony stimulating factors (G-CSF). On



5 Poor visibility of treated metastases and osteoblastic metastases. 69-year-old man with metastatic prostate cancer on long term, third line hormonal therapy with abiraterone being evaluated for rising serum prostate specific antigen (PSA) levels. He has had an excellent response to 2 years of treatment with residual abnormalities in his bone marrow visible on T1-weighted (5A) and T2-weighted (5B with fat suppression) spinal images. No hyperintensity is seen on the b900 3D MIP (inverted scale) image (5C) indicating the absence of osteolytic disease. Bone scan (5D) shows a focal area of osteoblastic uptake in the intertrochanteric region of the left femur (arrow) which is not visible as a discrete region on the b900 3D inverted MIP image.

WB-DWI, bone marrow hypocellularity demonstrates decreased signal intensity on high b-value images with the increased visibility of the spinal cord (Fig. 3). Marrow hypercellularity presents as diffuse increases in signal intensity on high b-values [5, 6]. Changes in background bone marrow cellularity can affect the visibility of bone marrow metastases. Bony metastases can become less conspicuous against increasing background signal intensities when growth colony stimulating factor (G-CSF) is used to prevent chemotherapy induced neutropenia (Fig. 4). On the other hand, the detection of bone metastases is improved in bone marrow that is relatively hypocellular, for example in the older patient or after chemotherapy (Fig. 2).

Skeletal metastases detection

On WB-DWI, skeletal metastases appear as focal or diffuse areas of high signal intensity on high b-values (Figs. 2, 4, 5). It is, however, important to emphasize

that WB-DWI should not be performed nor interpreted in isolation but rather has to be considered as a valued adjunct to anatomical whole-body MRI and therefore needs to be interpreted in conjunction with conventional WB-MRI studies [13]. This assertion has been highlighted in a recent meta-analysis which demonstrated that the high sensitivity of WB-DWI to detect metastases was at the expense of specificity [3]. Causes for false-positive findings are bone marrow edema caused by fractures, osteoarthritis, infection, bone infarcts, vertebral hemangiomas, isolated bone marrow islands and bone marrow hyperplasia due to G-CSF (Fig. 4). However, many of these false-positive findings can be overcome by correlating high b-value DW images with ADC maps and anatomical sequences [5].

In contrast, causes for false-negative findings are low levels of bone marrow infiltration such as in smoldering multiple myeloma or when background bone marrow hyperplasia obscures the pres-

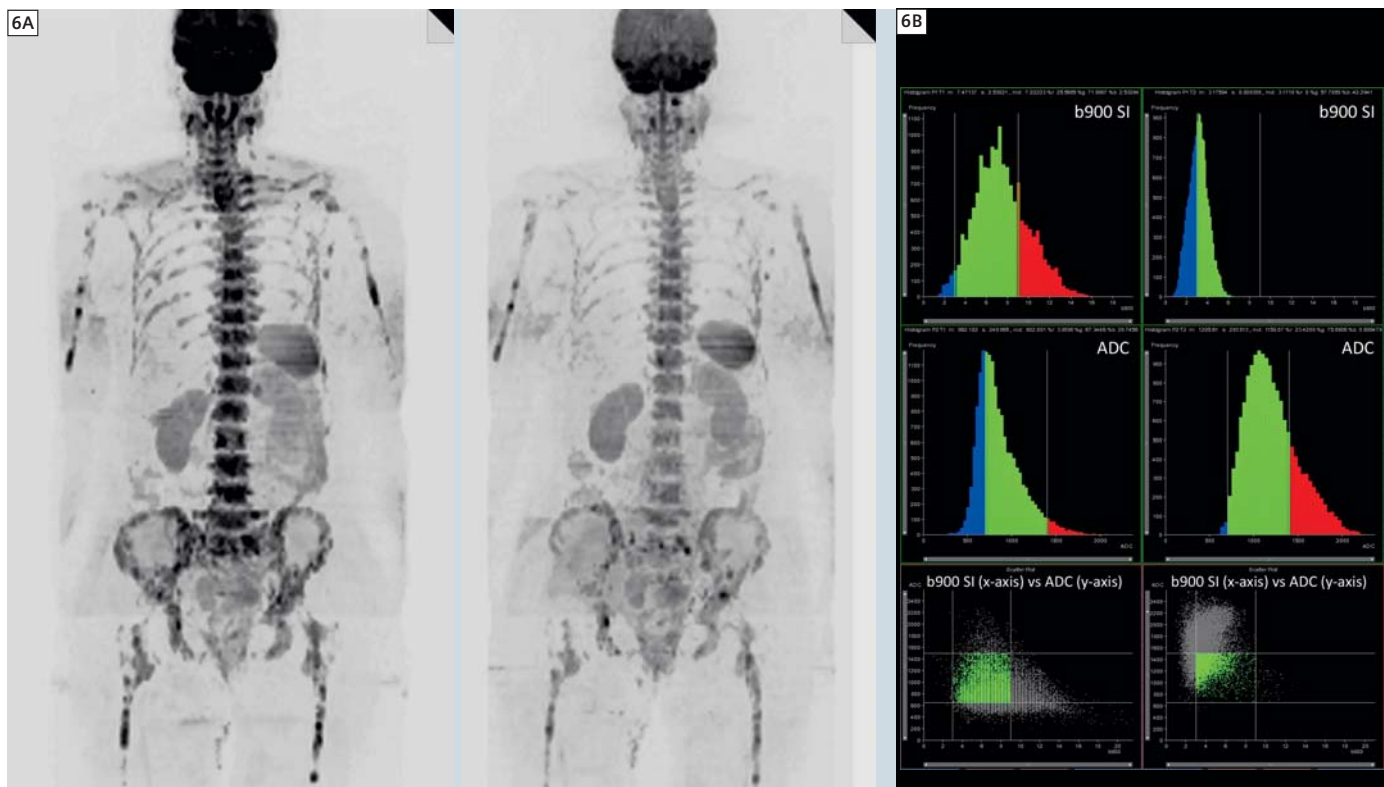
ence of metastases. Similarly, the detection of skeletal metastases on WB-DWI may be impaired in areas of macroscopic movement such as the anterior ribs and sternum. Visibility of skull vault infiltrations can be impaired because of the adjacent high signal of the brain. The visibility of skull base disease is impaired because of susceptibility effects. Another important cause for false-negative findings is successfully treated malignant disease and sclerotic metastases (Fig. 5). In general, lytic lesions are better detected than sclerotic or treated lesions on WB-DWI. This is due to the lower

water and cellular content of sclerotic and treated metastases [10, 14]. Diffusion-weighted MRI is better at detecting skeletal lesions from smaller cancer cell size infiltrations such as those due to breast cancer, myeloma, lymphoma and small cell tumors such as neuroendocrine tumors compared to bony metastases from clear cell cancers of the kidneys.

Therapy assessment of skeletal metastases on WB-DWI

Successful treatment of skeletal metastases is characterized by tumor cell death which results in increased water

diffusivity. On WB-DWI, this leads to marked increases of ADC values. The extent of ADC increases after successful therapy is thought to be related to mechanism of tumor cell death. It has been proposed that therapies which result in necrotic cell death may result in higher ADC values than treatment regimes which result in non-necrotic tumor cell death. This is thought to be due to the fact that necrotic cell death is associated with an inflammatory response which results in increased tissue water. Signal intensity changes on high b-values images after successful therapy are more



6 Therapy response in metastatic breast cancer. Serial changes in a 64-year-old woman with metastatic breast cancer responding to treatment with FEC (Fluorouracil (5FU), epirubicin and cyclophosphamide) chemotherapy with bisphosphonates. **(6A)** b900 3D MIP (inverted scale) images before (left column) and after 3 cycles of treatment (right column). A diffuse pattern of metastatic bone disease is seen pre-treatment that decreases in extent and signal intensity indicating disease response. There are a few focal areas of persistent signal hyperintensity post-therapy indicating likely active disease. **(6B)** Histogram analysis of a pelvic volume of interest defined on b900 images of the pre-treatment examination and applied to the second examination after robust image registration. Threshold histograms of muscle normalized b900 signal intensity (top row) and ADC values (middle row), and pixel scatter plots (bottom row) of normalized b900 signal intensity (x-axis) and ADC values (y-axis). The control lines on the histograms and scatter plots are placed on 3 and 9 for normalized b900 signal intensity and 650 and 1500 $\mu\text{m}^2/\text{s}$ for ADC values. The histograms show reductions in signal intensity (more blue pixels and less overall spread) on top row accompanied by increases in ADC values (more green and red pixels). Note how the pixel scatter plot moves to the top left. Analyses were done using OncoTreat* software (Works-in-progress, Siemens Healthcare, Erlangen, Germany).

*This information about this product is preliminary. The product is under development and not commercially available in the U.S., and its future availability cannot be ensured.

varied, but in most cases decreases in signal intensity are seen (Fig. 6).

Occasionally, successful treatment response may demonstrate persistent high signal intensity on high b-value images but with an associated increase in ADC-values. This appearance is termed 'T2 shine-through' and is due to tumor necrosis. It is thus prudent to always correlate high b-value images with ADC values when interpreting WB-DWI in order to avoid misinterpreting persistent high signal intensity on high b-value images as non-responding disease. Another pattern is a decrease in signal intensity on high b-values associated with unchanged ADC values or slight decreases in ADC values. Our experience from comparison with CT examinations, Dixon images and anatomical MRI studies suggests that this pattern may be due to sclerosis or fibrosis. We have classified this pattern as indeterminate and therefore take into account other radiological and clinical findings for response assessment. By contrast, patients who fail to respond to therapy usually demonstrate persistent or increasing bone marrow hyperintensity on high b-value images. In the context of disease progression, a decrease or no change in ADC values can be observed because of increasing in tumor cell density within the confines of a fixed bone marrow space. Small increases in ADC values can also be observed in progressive disease (but of a much smaller magnitude compared to responding lesions). For this reason we use an upper ADC cut-off value derived from untreated patients in order to differentiate responders from non-responders. This cut-off value is likely to be dependent on the choice of b-values utilized and the tumor type [5, 6].

Clinical indications

At our institution, we have performed more than 1,200 WB-MRI examinations incorporating diffusion MRI in the last four years using it for bone marrow metastasis detection and therapy monitoring for a variety of cancer types – principally in breast and prostate cancer and multiple myeloma. It is increasingly

being used for the evaluation of patients with melanoma, lymphoma and renal cancer. We have also found it valuable for the examination of children* and young adults, pregnant* women with cancer and in patients with impaired renal function or allergies when there is a contraindication to the intravenous injection of contrast medium.

Conclusions

WB-DWI has emerged as a powerful imaging tool in the detection, characterization and for monitoring of treatment response of tumors. It particularly excels in the detection and disease extent assessment of bone marrow lesions as well as in the evaluation of therapy response of skeletal lesions. It is however important to emphasize the fact that WB-DWI has to be interpreted in conjunction with conventional whole-body MRI sequences in order to avoid pitfalls in diagnoses. There is an urgent need to better understand the biologic basis of treatment-related changes. Furthermore response criteria need to be established and tested in prospective clinical studies. Nevertheless, WB-DWI demonstrates great potential in the evaluation of bone marrow lesions because it is quick to perform, can be incorporated into standard clinical protocols and can potentially answer clinical questions regarding tumor response more reliably than conventional imaging modalities.

*MR scanning has not been established as safe for imaging fetuses and infants under two years of age. The responsible physician must evaluate the benefit of the MRI examination in comparison to other imaging procedures.

Contact

Prof. Anwar R. Padhani, MBBS FRCP FRCR
Paul Strickland Scanner Centre
Mount Vernon Cancer Centre
Rickmansworth Road
Northwood
Middlesex HA6 2RN
United Kingdom
Phone: +44-(0) 1923-844751
Fax: +44-(0) 1923-844600
anwar.padhani@stricklandscanner.org.uk

References

- Jadvar H. Prostate cancer: PET with 18F-FDG, 18F- or 11C-acetate, and 18F- or 11C-choline. *J Nucl Med* 2011;52:81-89.
- Mankoff DA, Link JM, Linden HM, Sundarajan L, Krohn KA. Tumor receptor imaging. *J Nucl Med* 2008;49 Suppl 2:149S-163S.
- Wu LM, Gu HY, Zheng J, et al. Diagnostic value of whole-body magnetic resonance imaging for bone metastases: a systematic review and meta-analysis. *J Magn Reson Imaging* 2011;34:128-135.
- Schmidt GP, Reiser MF, Baur-Melnyk A. Whole-body MRI for the staging and follow-up of patients with metastasis. *Eur J Radiol* 2009;70:393-400.
- Padhani AR, Koh DM, Collins DJ. Whole-body diffusion-weighted MR imaging in cancer: current status and research directions. *Radiology* 2011;261:700-718.
- Padhani AR, Gogbashian A. Bony metastases: assessing response to therapy with whole-body diffusion MRI. *Cancer Imaging* 2011;11 Spec No A:5:129-145.
- Padhani AR. Diffusion magnetic resonance imaging in cancer patient management. *Semin Radiat Oncol* 2011;21:119-140.
- Koh DM, Blackledge M, Padhani AR, et al. Whole-Body Diffusion-Weighted MRI: Tips, Tricks, and Pitfalls. *AJR Am J Roentgenol* 2012;199:252-262.
- Hwang S, Panicek DM. Magnetic resonance imaging of bone marrow in oncology, Part 1. *Skeletal Radiol* 2007;36:913-920.
- Messiou C, Collins DJ, Morgan VA, Desouza NM. Optimising diffusion weighted MRI for imaging metastatic and myeloma bone disease and assessing reproducibility. *Eur Radiol* 2011;21:1713-1718.
- Hillengass J, Bauerle T, Bartl R, et al. Diffusion-weighted imaging for non-invasive and quantitative monitoring of bone marrow infiltration in patients with monoclonal plasma cell disease: a comparative study with histology. *Br J Haematol* 2011;153:721-728.
- Nonomura Y, Yasumoto M, Yoshimura R, et al. Relationship between bone marrow cellularity and apparent diffusion coefficient. *J Magn Reson Imaging* 2001;13:757-760.
- Lecouvet FE, El Mouedden J, Collette L, et al. Can whole-body magnetic resonance imaging with diffusion-weighted imaging replace Tc 99m bone scanning and computed tomography for single-step detection of metastases in patients with high-risk prostate cancer? *Eur Urol* 2012;62:68-75.
- Eiber M, Holzapfel K, Ganter C, et al. Whole-body MRI including diffusion-weighted imaging (DWI) for patients with recurring prostate cancer: Technical feasibility and assessment of lesion conspicuity in DWI. *J Magn Reson Imaging* 2011;33:1160-1170.